Hindawi
Journal of Nanomaterials
Volume 2021, Article ID 9619256, 14 pages
https://doi.org/10.1155/2021/9619256

Research Article

Electrochemical Behavior and Electronucleation of Copper Nanoparticles from $CuCl_2{\cdot}2H_2O$ Using a Choline Chloride-Urea Eutectic Mixture

Thao Dao Vu Phuong,[1,2] Thuy-Linh Phi,[1] Bui Huu Phi,[1] Nguyen Van Hieu,[3,4] Son Tang Nguyen,[5] and Tu Le Manh[1,2]

[1]*Faculty of Materials Science and Engineering, Phenikaa University, Hanoi 12116, Vietnam*
[2]*Advanced Institute for Science and Technology (AIST), Hanoi University of Science and Technology (HUST), No 01, Dai Co Viet Road, Hanoi, Vietnam*
[3]*Phenikaa Research and Technology Institute (PRATI), A&A Green Phoenix Group, 167 Hoang Ngan, Hanoi 100000, Vietnam*
[4]*Faculty of Electrical and Electronic Engineering, Phenikaa Institute for Advanced Study, Phenikaa University, Yen Nghia, Ha-Dong District, Hanoi, Vietnam*
[5]*Faculty of Biotechnology, Chemistry and Environmental Engineering, Phenikaa University, Hanoi 10000, Vietnam*

Correspondence should be addressed to Son Tang Nguyen; son.nguyentang@phenikaa-uni.edu.vn
and Tu Le Manh; tu.lemanh@phenikaa-uni.edu.vn

Received 4 May 2021; Revised 18 June 2021; Accepted 3 July 2021; Published 19 July 2021

Academic Editor: Thanh Dong Pham

This work presents a thorough study on the early stage of copper electrodeposition from a choline chloride-urea deep eutectic solvent (DES). Determination of possible species in DES containing Cu^{2+} ions as the electrolytes has been performed using UV-Vis measurements. Kinetic and thermodynamic aspects of copper electrodeposition on glassy carbon electrode from DES were thoroughly investigated using cyclic voltammetry (CV) and chronoamperometry (CA). Both results from CA and CV have demonstrated that the copper electrodeposition could be performed directly from DES containing a small amount of water by the single potentiostatic step technique. Theoretical approach confirmed that the direct electronucleation of copper nanoparticles in the DES can be described by a model with two contributions, namely, (i) adsorption process and (ii) a three-dimensional (3D) nucleation and diffusion-controlled growth of copper nuclei, to the total current density transients. Kinetic parameters are important for controlling morphology and chemical composition of the obtained nanoparticles, which are verified by surface characterization techniques such as SEM and EDS.

1. Introduction

Copper nanoparticles (Cu-NPs) are of great interest for applications in many engineering fields, including electronics, energy, catalyst, environment, and agriculture, owing to their natural abundance, low cost, and diversity of preparation methods [1, 2]. Some (typical) examples can be mentioned such as the use of Cu-NPs in sensors [3], fuel cell, and solar cell [4, 5] and in conductive inks for printed electronics [6]. In agriculture, Cu-NPs have also shown important effect in regulating plant growth and development and increasing chlorophyll formation and seed production [7]. Moreover, due to their fungicidal and insecticidal activity against the pests of crop plants, they can be used as nano-pesticides, nano-herbicides, nano-fertilizers [8, 9], among others. These benign behaviors of Cu-NPs make the study on their synthesis a topic of current interest.

It is known that Cu-NPs can be produced by different routes, physical methods, or chemical methods [10]. The main concern is the fact that these methods are neither cost-effective nor eco-friendly due to the use of toxic

chemicals [11]. The electrochemical synthesis of Cu-NPs from a "green" solvent such as a deep eutectic solvent (DES) based on choline chloride could be a promising candidate to tackle these problems.

DESs have received much attention for metals electrodeposition applications (i.e., Ni, Fe, Al, and Zn [12–16]) due to several advantages, such as a wide electrochemical window, low cost, ease of preparation, negligible vapor pressure, thermal stability, and (nearly) null hydrogen liberation during electrodeposition [17, 18], compared to conventional aqueous solvents. Particularly, in the case of copper, although the copper electrodeposition from DESs has been reported in the literatures [19, 20], insights on the early stages of this process, specifically, mechanistic and kinetic aspects, are still limited. Abbott et al. [19] have first studied the copper electrodeposition in the eutectic mixture of choline chloride and ethylene glycol (ethaline) and found that copper reduction occurs via two well separated one-electron stages: Cu(II)-Cu(I)-Cu. These processes have been studied by Sebastián et al. [20] using Cu(I) and Cu(II) solutions dissolved in aqueous solvent and in the mixture of choline chloride and urea (reline), DES. They proposed the use of the double potentiostatic step technique to separate current densities related to the reduction of each copper species. However, there have been some concerns in the application of this technique and unsolved problems as follows: (i) it can be facilitated in a medium with the low mobility of species (such as the reline DES under their studied conditions), but it is difficult in medium with the good mobility of ionic species (i.e., aqueous medium); (ii) success of the procedure is dependent on control of the initial conditions at which electrodeposition takes place [20], (iii) effect of residual water in DES has not been considered, while several recent papers [21, 22] have reported that a small amount of water can influence physiochemical properties, the dynamics, and the electrochemistry of active species, (i.e., decreasing the viscosity and resistivity of the DES and altering the speciation of the copper chloro-complexes) [22, 23]; and (iv) although Sebastian et al. [20] have reported some initial results on the copper electronucleation in DES using cyclic voltammetry (CV) and chronoamperometry (CA), insights on the mechanisms and kinetics including mathematical models capable of describing the Cu nucleation and growth processes from DES in practical conditions where it can contain some unavoidable small amounts of residual water adsorbed from the environment or DES preparation, and some important kinetic parameters such as the nucleation frequency, A, the number density of active sites for copper nucleation onto the electrode surface, N_0, have been not determined. Consequently, the knowledge on these aspects must be updated; in addition, (v) details on the speciation of copper ions dissolved in DES and the possibility of using the conventional potentiostatic method to electrodeposit copper from DES have not yet been studied.

Therefore, the aim of this work is to study the nucleation and growth mechanisms and kinetics of copper deposition process on glassy carbon electrode from the reline containing Cu^{2+} ions as the electrolyte solution using both theoretical and experimental approaches. UV-Vis spectra were used to analyze the species containing in Cu^{2+} electrolyte solution.

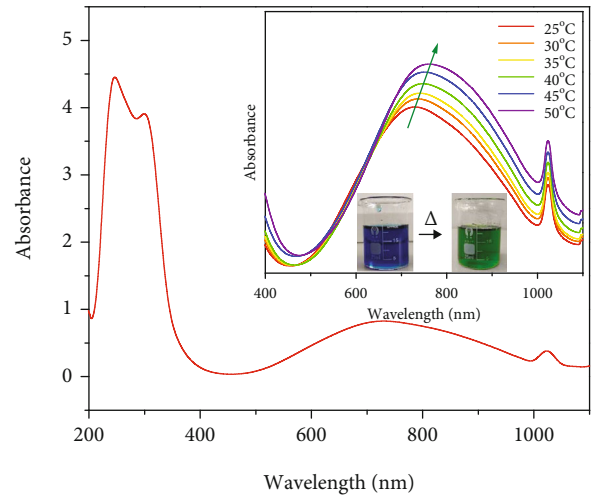

FIGURE 1: UV-Vis-NIR spectra of 10 mM of $CuCl_2{\cdot}2H_2O$ in reline at different temperatures. The inset depicts the shift to the right-hand side of the NIR region, indicating the color change recorded in the system.

2. Materials and Methods

2.1. DES and Electrolyte Preparation. Chemicals such as choline chloride ($C_5H_{14}ClNO$, 97%, Sigma-Aldrich), urea (CH_4N_2O, 99%, Sigma-Aldrich), and copper (II) chloride hexahydrate ($CuCl_2{\cdot}2H_2O$, ACS reagent, ≥99.0%) were used. DES was prepared by mixing choline chloride and urea in a 1 : 2 molar ratio at 100°C. This obtained mixture was constantly stirred until a transparently homogenous solution was obtained. Details of DES preparation can be found in our previous study [24]. The Cu^{2+} electrolyte solution was obtained by adding 50 mM copper (II) chloride hexahydrate salt, to the DES, and the solution was stirred for 12 hours at 60°C. The obtained electrolyte solution was kept in a dehumidifier for latter electrochemical measurements. The water content of $CuCl_2{\cdot}2H_2O$ dissolved in DES was measured by Karl Fischer coulometric titration, using a Titrino Coulometer (Model 756, Metrohm), giving a value of about 0.35%.

2.2. UV-Vis Measurements. UV-Vis measurements of the electrolytes containing Cu(II) dissolved in DES were performed in an UV-Vis spectrophotometer (UV-6850, JENWAY Double Beam Spectrophotometer). UV-Vis spectra of the solution were obtained for different temperature (25°C to 50°C) in a quartz cell with a light path length of 1.0 cm using the Prism 5.51 PC software coupled to the equipment.

2.3. Electrochemical Tests. A conventional water-jacketed cell comprising three electrodes was used for CV and CA tests. The electrochemical cell was composed of a glassy carbon electrode (GCE), with 0.0707 cm^2 surface area as the working electrode, a platinum wire, and a silver wire as counter and

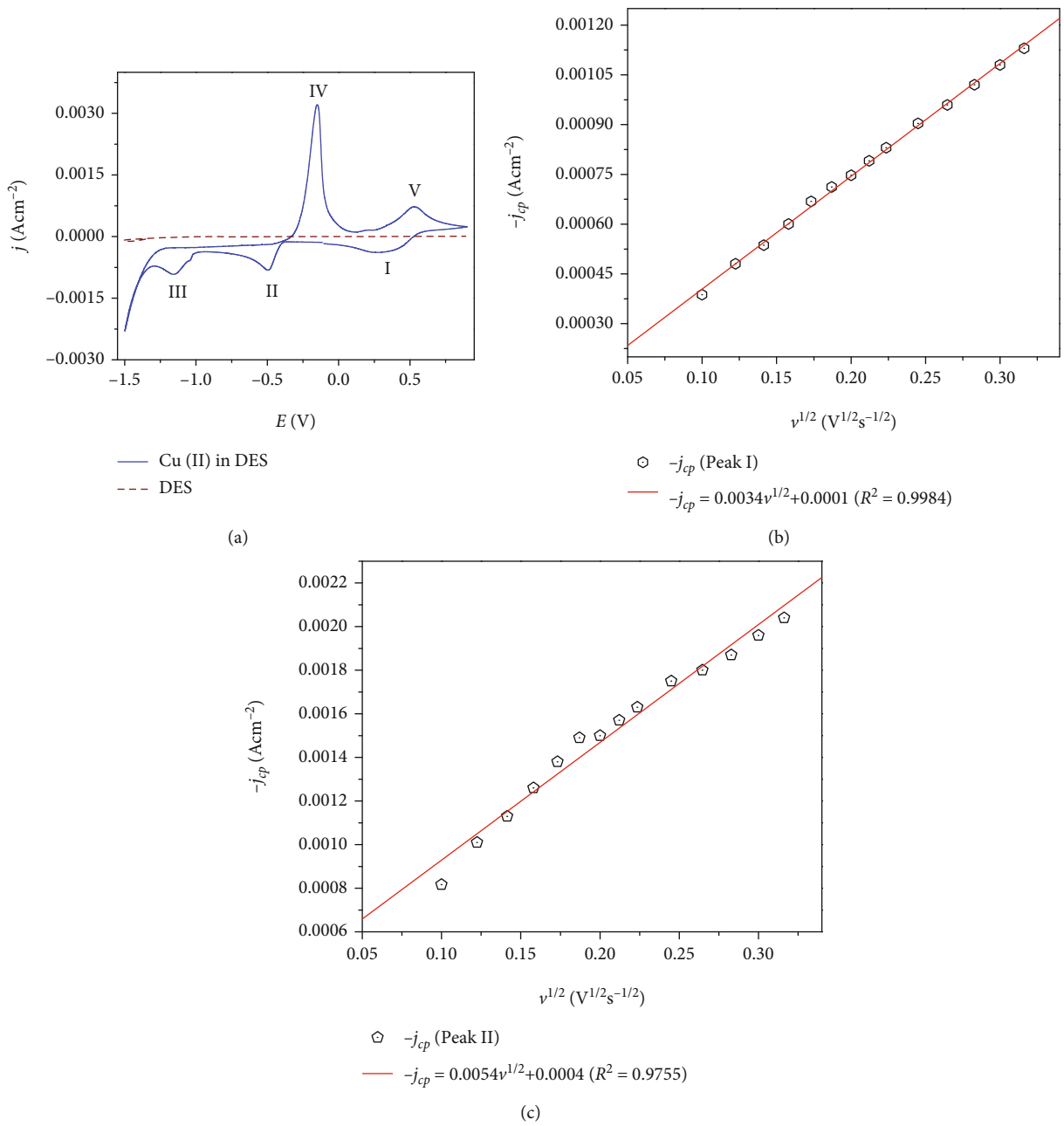

Figure 2: Continued.

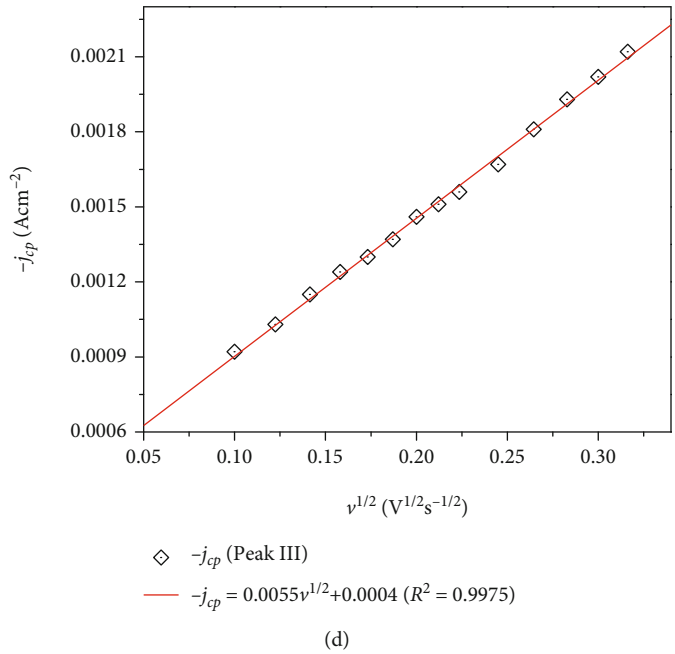

FIGURE 2: (a) CVs obtained in the system GCE/DES (discontinuous curve) and GCE/50 mM Cu(II) in DES (blue curve) at 70°C. The scan was started at a potential of 0.40 V in the negative direction with a scan rate of 10 mVs^{-1}. CVs recorded onto GCE using different scan rates and cathodic peak current density (j_{cp}) as a function of the scan rate ($v^{1/2}$) at 70°C for (b) peak I, (c) peak II, and (d) peak III.

quasi reference electrode, respectively. The electrochemical cell temperature was controlled by a Lauda RMS 179 Circulator with RM6 Refrigerating Water Bath Chiller, −15 to 100°C (with a temperature stability of ±0.02°C). CA and CV measurements were carried out using VersaStat 3 system, coupled to the VersaStudio software installed in a PC for experimental control and data collection. These experiments were performed at 70°C.

2.4. Surface Analysis Characterization. Morphological and chemical compositions of the electrodeposits were characterized using field emission scanning electron microscope (FE-SEM), Model JEOL JSM SEM 7000F, and energy-dispersive X-ray spectroscopy (EDS), respectively, to confirm the existence of Cu-NPs on the GCE surface.

3. Results and Discussion

3.1. Copper Speciation in the Reline. A drastic change in color of Cu^{2+} ions dissolved in DES from blue to green before and after heating (see Figure 1) can be observed with the naked eyes. The green color of the Cu^{2+} electrolyte solution remains unchanged and becomes stable after heating. This phenomenon is able to be recorded by UV-Vis spectra as shown in Figure 1. It reveals two peaks in the UV region, at 246 nm and 298 nm, which can be assigned to the presence of species such as $[CuCl_4]^{2-}$ [25]. Meanwhile, in the near infrared (NIR) region, a broader peak between from 705 to 755 nm and a sharp peak at 1022 nm are detected, which can be due to the presence of $[Cu(H_2O)_6]^{2+}$ species [26]. By increasing the temperature, the absorbance peaks tend to shift to higher value of wavelength (inset of Figure 1). These results confirm the presence of different complexes in DES such as $[Cu(H_2O)_6]^{2+}$ and $[CuCl_4]^{2-}$ species corresponding to room temperature and higher temperature, respectively. Thus, at room temperature, $[Cu(H_2O)_6]^{2+}$ can be predominant due to the small amount of residual water in DES, which is due to the use of $CuCl_2{\cdot}2H_2O$ salt and/or atmospheric moisture. After heating, this water tends to evaporate, and Cl^- ions can substitute (partially) the H_2O ligands to form $[CuCl_4]^{2-}$ complexes. The color change of $CuCl_2$ solution in choline chloride-based DESs has been also observed in other studies [22, 26], where $CuCl_2$(hyd.) dissolved in ethaline exhibits yellow color, typical of forming $[CuCl_4]^{2-}$ species, and by adding water to the solution it shifts from yellow to blue. According to Valverde et al. [22] and Vreese et al. [26], this color change can be explained due to the substitution of Cl^- by H_2O ligand. Therefore, the general species of $CuCl_2{\cdot}2H_2O$ dissolved in reline could be presented in form of the mixed chloro-aqua chemical complex structure $[CuCl_n(H_2O)_m]^{(2-x)-}$, where $n + m = 4 \longrightarrow 6$ and $x = 0 \longrightarrow 6$ [22, 26].

3.2. CV Study. Figure 2(a) shows the CVs recorded on the GCE in DES (discontinuous curve of Figure 2(a)) and with 50 mM Cu^{2+} ions dissolved in DES at 70°C. It can be seen that the (current density) contribution of the pure DES is insignificant and can be neglected. Several peaks (I, II, IV, and V) observed in Figure 2(a) correspond to different electrochemical reactions of Cu^{2+} in DES occurring on the GC electrode surface. In the forward scan of the CV, three reduction peaks are clearly observed in the potential ranges from 0.6 V to -0.1 V (peak I), -0.4 V to -0.86 V (peak II), and from -1.0 V to -1.30 V (peak III).

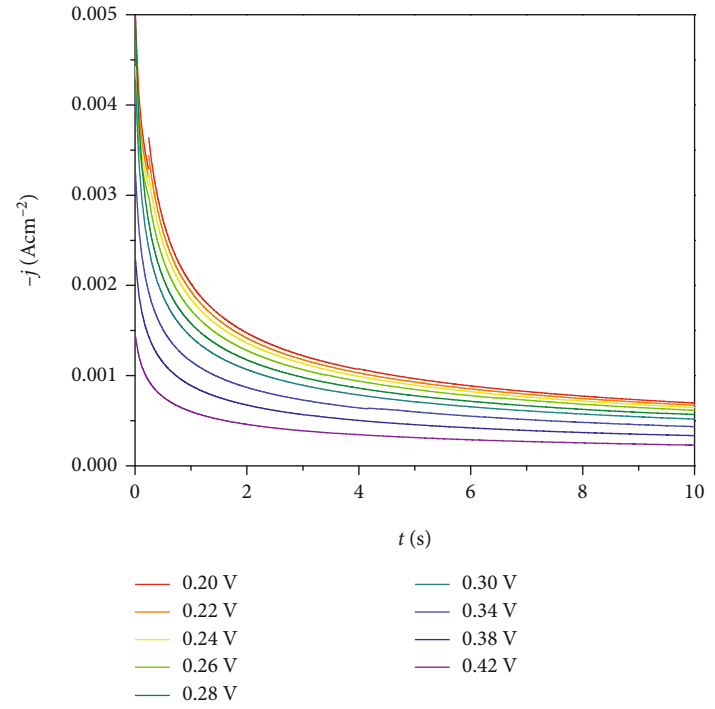

(a)

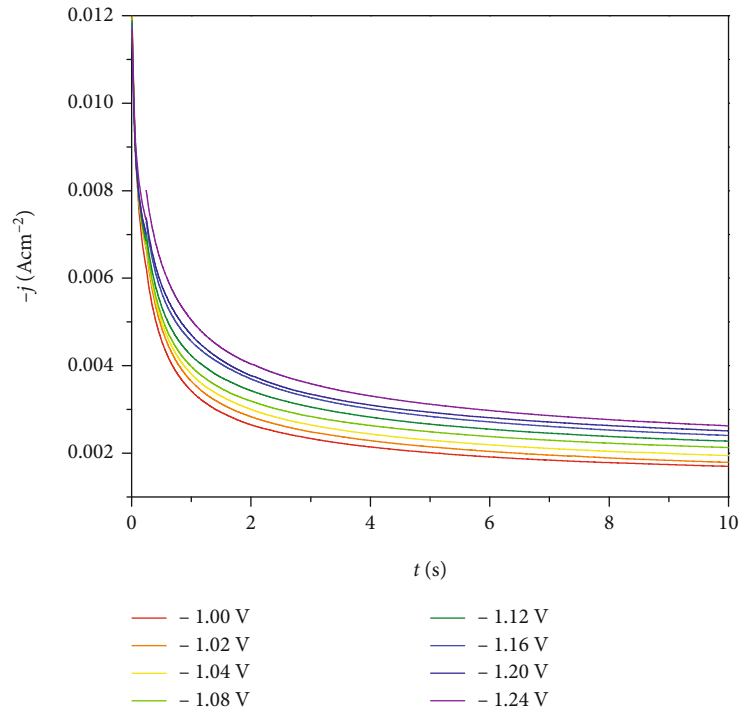

(b)

Figure 3: Continued.

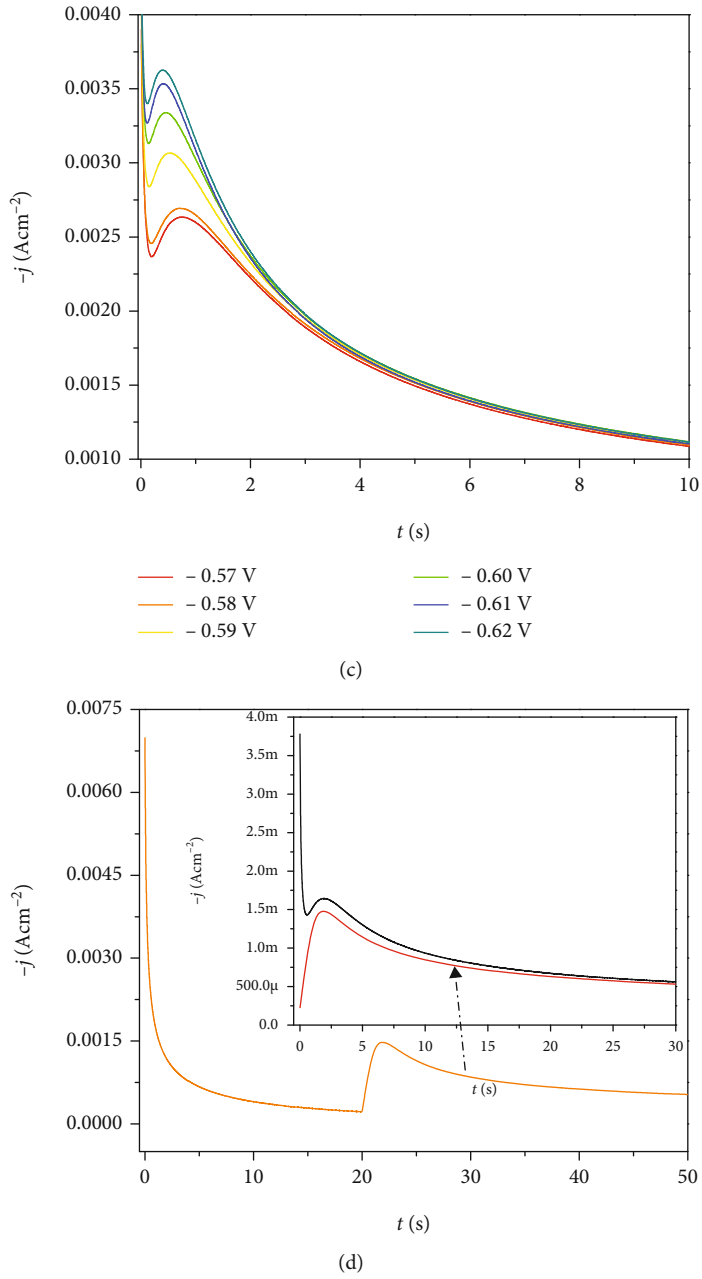

FIGURE 3: CAs recorded in the system GCE/50 mM Cu(II) in DES at 70°C using different potentials located at the region closed to (a) peak I, (b) peak III, and (c) peak II, defined by the CV depicted in Figure 2(a), and (d) comparison between the experimental CAs at -0.52 V using single potential step and double potential step (applying first step from -0.1 V, then the second step -0.52 V (red line) as shown in the inset).

According to Sebestian et al. [20], the first two peaks can be assigned to the transition process from Cu^{2+} to metallic Cu associated with the reactions, (1) and (2):

$$Cu^{2+}{}_{DES} + e - \longrightarrow Cu^{+}{}_{DES} \quad (1)$$

$$Cu^{+}{}_{DES} + e^{-} \longrightarrow Cu_{(s)} \quad (2)$$

The water reduction reaction to hydrogen associated with peak III observed in the CV (Figure 2(a)) can be given by (3) [23]:

$$2H_2O_{DES} + 2e^{-} \longrightarrow H_2 + 2OH^{-} \quad (3)$$

Meanwhile, in the backward scan, the oxidation peak located in the potential range of -0.40 V to 0.05 V can be attributed to the oxidation reaction of Cu metallic nuclei

(see (4)) previously formed by (2) during the forward scan. The other peak located at 0.28 V–0.80 V (peak V) can be associated with the oxidation reactions of Cu^{+}_{DES} from (1), as given in (5).

$$Cu_{(s)} \longrightarrow Cu^{+}_{DES} + e^{-} \quad (4)$$

$$Cu^{+}_{DES} \longrightarrow Cu^{2+}_{DES} + e^{-} \quad (5)$$

At potentials larger than the potential ranges of peaks III and V, at the extremes of the CV, the current intensity growths are known as the decomposition reactions (reduction and oxidation, respectively) of the solvent [17, 27]. Since this work deals with the copper electronucleation, the reduction reactions, such as (1) and (2), are paid more attention.

To investigate the electrochemical behavior of the system GCE/50 mM Cu(II) in DES, CVs are carried out at different scan rates ranging from 10 to 100 mVs^{-1}. It reveals that cathodic peak current density (j_{cp}) increments with as the scan rate increases. By plotting j_{cp} as a function of square root of the scan rate ($v^{1/2}$) for three peaks I, II, and III (see Figures 2(b)–2(d)), it can be clearly seen that j_{cp} of these peaks exhibits a linear relationship with $v^{1/2}$. This means that the Cu electrodeposition on GCE from DES follows a diffusion-controlled mechanism, which can be described by the Berzins-Delahay equation [28]:

$$j_{cp} = \frac{0.61 \times (Fn)^{3/2} C_0 (Dv)^{1/2}}{(RT)^{1/2}}, \quad (6)$$

where F is the Faraday constant, R is the ideal gases constant, n is the total number of electrons transfer, C_0 (mol cm^{-3}) is the bulk concentration of reduced species, D ($cm^2\,s^{-1}$) is the diffusion coefficient of Cu(II) ions, and T (K) is the temperature of medium.

According to the CV, copper electrodeposition mechanism must be occurred in two steps through (1) and (2). Therefore, from peaks I and II of interest, there are two values of diffusion coefficient to be determined, D_I and D_{II}, correspondingly. D_I can be calculated from Eq. (6) and using the slopes of Figure 2(b) and the initial concentration $C_0 = 0.05$ M; thus, $D_I = 9.9536 \times 10^{-8}\,cm^2\,s^{-1}$. D_{II} is more difficult to determine since Cu^{+} concentration is unknown. Fortunately, in the same DES, concentration, and working temperature, Sebastian et al. [29] have proposed a methodology to estimate the surface concentration (C_s) of Cu^{+} ions using the double step technique, which yields $C_s = 0.01694$ M. Taking into account the C_s and the slope values of Figure 2(c), from Eq. (6), it can be derived $D_{II} = 8.67 \times 10^{-7}\,cm^2\,s^{-1}$ for peak II. These values are consistent with those reported by Sebastian et al. [20] and Popescu et al. [30]. A significant increase in the value of D from peak I to peak II can be explained due to the transition from species Cu^{2+} to Cu^{+} (see (1)) as D is inversely proportional to their atomic radius. This follows the Stokes-Einstein equation as discussed by Mejia-Caballero et al. [31] in the case of chromium.

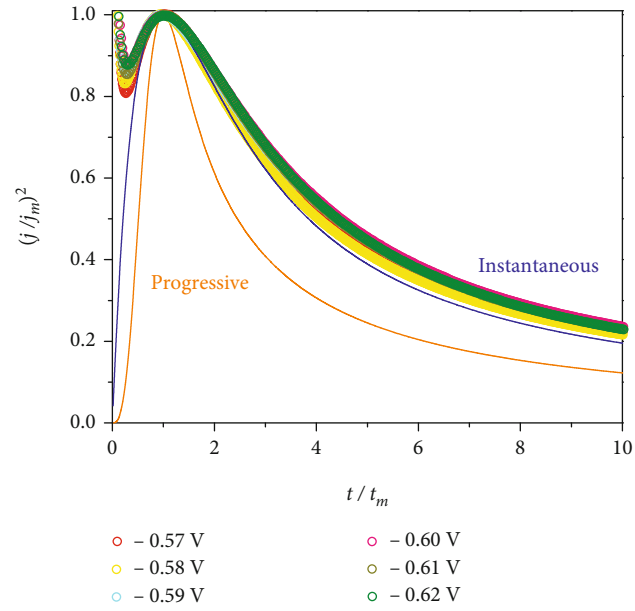

Figure 4: Comparison of the nondimensional plots of the experimental CAs (scatter line) depicted in Figure 3(c) with the theoretical ones for instantaneous (blue) and progressive (orange) nucleation.

3.3. Potentiostatic Study. Figure 3 depicts CA curves recorded on the GCE at 70°C using the potential range defined from CV (Figure 2(a)). In general, a clear distinction of nucleation mechanisms can be observed from CAs of the studied reduction peaks. Figures 3(a) and 3(b) depict the CAs with a typical Cotrellian behavior, while the CA shapes of Figure 3(c) suggest that the early stage of the Cu electrodeposition onto GCE from DES could follow the three-dimensional (3D) nucleation and diffusion-controlled growth [32]. This demonstrates that direct electrodeposition of copper from DES is evident by simply using the single potential step. The direct electrodeposition of copper in this work refers to the single potential step or the conventional chronoamperometry, by applying only one potential pulse to deposit copper from Cu^{2+} to Cu, as be illustrated by the following mechanism, (7):

$$Cu^{2+} + e^{-} <=> Cu^{+} + e^{-} <=> Cu \quad (7)$$

In difference with Sebastian et al. [20], who have stated that (7) could be difficult, Figure 3(d) clearly indicates that both (single and double pulse) techniques can be performed successfully to electrodeposit copper from DES in our case. Interestingly, while the double potentiostatic steps can separate the reduction reactions of each copper species, the single pulse seems to be more advantageous by shortening the reaction time of (1), transition from Cu^{2+} to Cu^{+}, which results in a more complex shape of the experimental CA with an additional (adsorption) contribution to the total current transient density. This process can be explained due to the presence of the residual water containing in the DES, which significantly influences

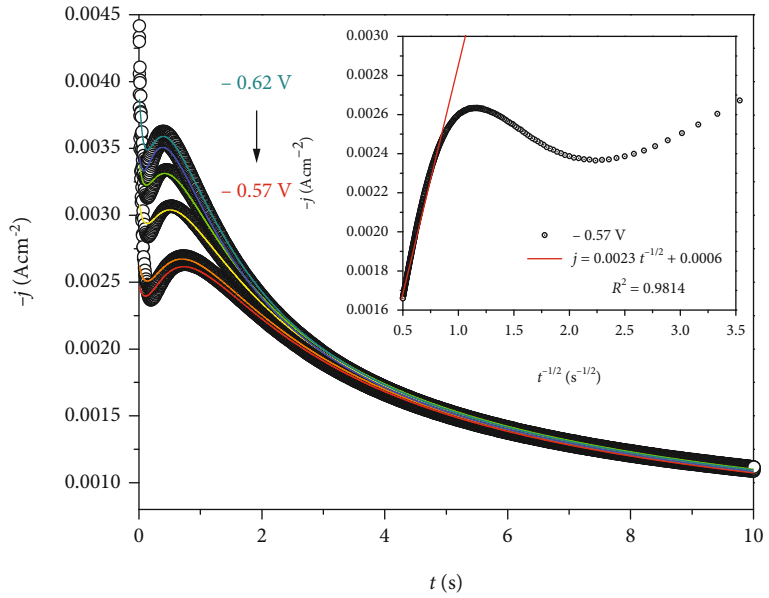

Figure 5: Comparison between the CAs (circle) (lines) recorded in the system GC/50 mM $CuCl_2$ in DES at the potentials (from -0.57 to -0.62 V with a step = −0.01 V), and the theoretical transients (line) obtained after fitting Eq. (12) to the experimental data. The inset of Figure 5 illustrates the Cottrell analysis ($j - t^{-1/2}$ plot) of the CA at -0.57 V.

Table 1: Best-fit parameters obtained from fitting Eq. (12) to the experimental data.

$-E$ (V)	$10^3 P_1$ (A $s^{1/2}$ cm^{-2})	P_2 (s^{-1})	A (s^{-1})	$10^3 P_4$ (Acm^{-2})	P_5 (s^{-1})	$10^{-6} N_0$ (cm^{-2})	$10^7 D$ (cm^2 s^{-1})	$10^{-7} AN_0$ (s^{-1} cm^{-2})
0.57	3.394 ± 0.002	1.065 ± 0.093	4.031 ± 0.072	2.492 ± 0.028	1.267 ± 0.158	9.232 ± 0.806	3.889 ± 0.005	3.722 ± 0.075
0.58	3.424 ± 0.002	1.143 ± 0.071	3.894 ± 0.079	2.647 ± 0.021	1.391 ± 0.132	9.741 ± 0.605	3.956 ± 0.005	3.793 ± 0.081
0.59	3.463 ± 0.002	1.346 ± 0.081	4.902 ± 0.123	3.117 ± 0.020	1.668 ± 0.148	11.217 ± 0.667	4.047 ± 0.005	5.499 ± 0.141
0.60	3.482 ± 0.002	1.533 ± 0.102	5.594 ± 0.128	3.428 ± 0.024	1.880 ± 0.174	12.632 ± 0.840	4.091 ± 0.005	7.066 ± 0.166
0.61	3.428 ± 0.002	1.746 ± 0.146	6.899 ± 0.126	3.486 ± 0.030	2.102 ± 0.235	14.846 ± 1.241	3.966 ± 0.005	10.242 ± 0.196
0.62	3.463 ± 0.002	2.519 ± 0.058	6.578 ± 0.461	3.982 ± 0.025	3.540 ± 0.261	20.976 ± 0.483	4.049 ± 0.005	13.799 ± 0.967

the dynamics and the electrochemistry of active species as shown in Figure 1.

Paying attention to peak II, Figure 3(c) reveals that the peak current densities of the system GCE/Cu^{2+} in DES increase with the increase of the applied potentials. For the determination of the governed nucleation types (instantaneous or progressive nucleation) in the Cu electrodeposition process onto the GCE, a nondimensional analysis is performed using the theoretical plots, which are well-known as Scharifker and Hills models [33].

$$\left(\frac{j}{j_m}\right)^2 = 1.9542\left(\frac{t}{t_m}\right)^{-1}\left(1-\exp\left[-1.2564\left(\frac{t}{t_m}\right)\right]\right)^2,$$
$$\left(\frac{j}{j_m}\right)^2 = 1.2254\left(\frac{t}{t_m}\right)^{-1}\left(1-\exp\left[-2.3367\left(\frac{t}{t_m}\right)^2\right]\right)^2. \quad (8)$$

Figure 4 reveals that at 70°C, for $t/t_m \leq 0.7$ and $t/t_m \geq 2.1$, the nondimensional plots of the experimental current density transients are above the instantaneous one, which is out of the validated zone of the 3D nucleation and diffusion-controlled growth [33]. According to [31], the classic form of the Scharifker and Mostany (SM) model is not applicable, and a modified one based on the SM could be convenient.

Table 2: Diffusion coefficient calculated using the Cottrellian behavior (see the parameter P_1 in Eq. (9)) for different reduction peaks.

Cottrell analysis	Peak I	Peak II
$10^7 D$ (cm^2 s^{-1})	2.0452	7.9493

The parametric form of the SM model associated with the 3D nucleation and growth is given by [31]:

$$j(t)_{3D} = P_1 t^{-1/2}\left(1-\exp\left\{-P_2\left[t-\frac{1-\exp\left(-P_3 t\right)}{P_3}\right]\right\}\right), \quad (9)$$

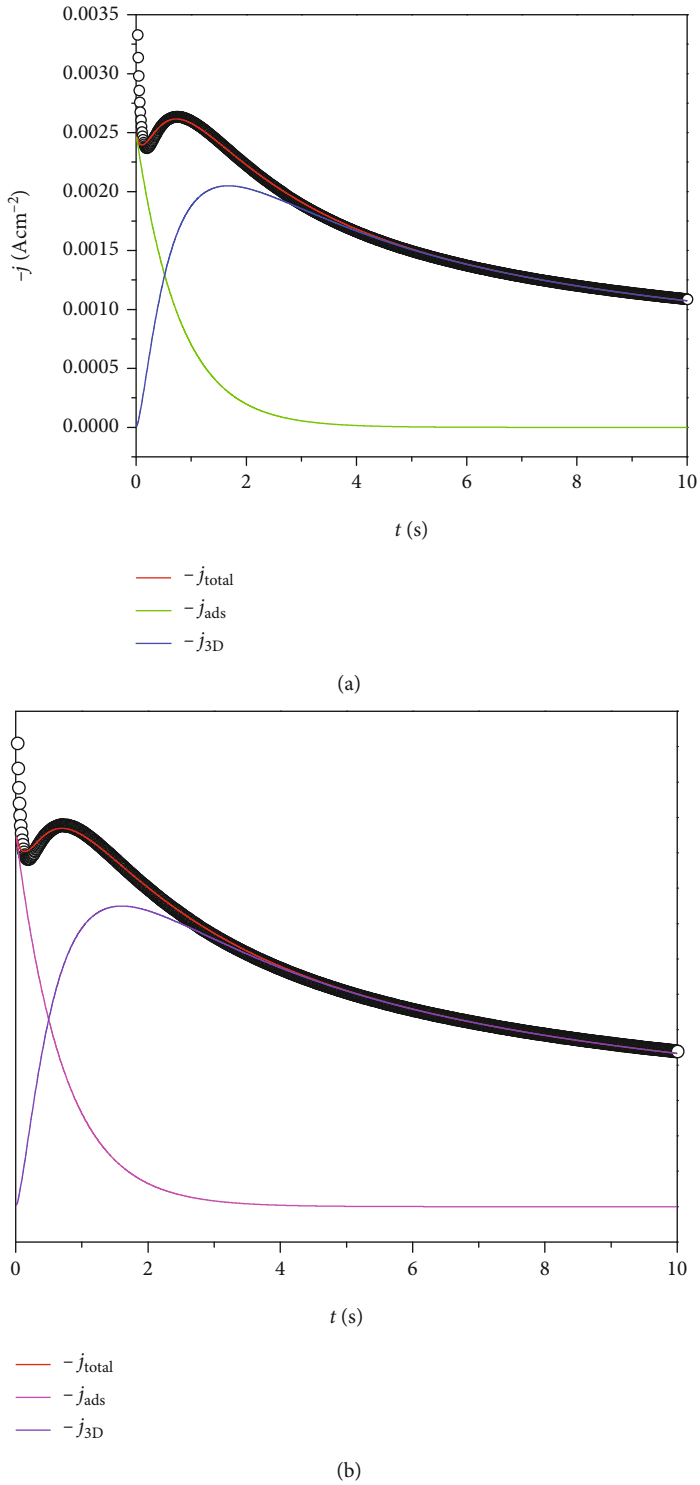

FIGURE 6: Separation of individual contributions to the total current density transient using Eq. (12) for different applied potentials: (a) -0.57 V; (b) -0.58 V.

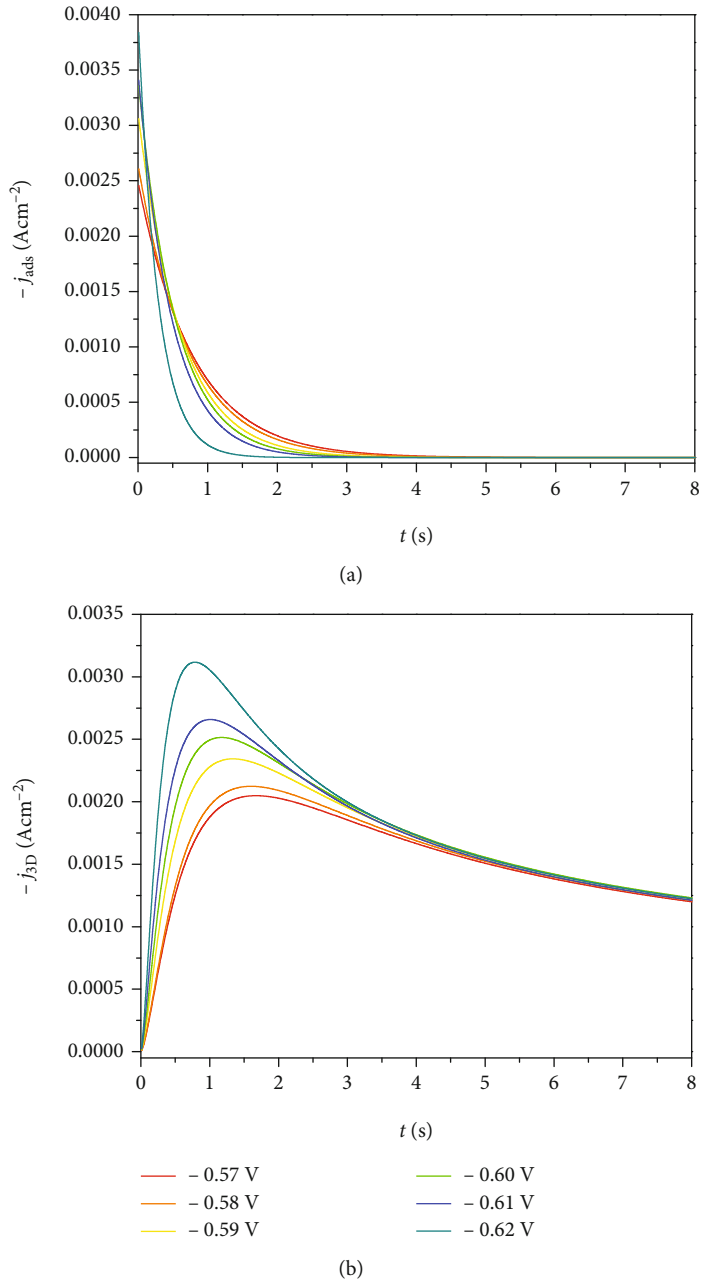

FIGURE 7: Individual contributions of adsorption and 3D nucleation derived from Eq. (12) for CA curves obtained in Figure 5.

where

$$P_1 = \frac{z\mathrm{F}\mathrm{D}^{1/2}C_0}{\pi^{1/2}},$$
$$P_2 = N_0\pi D\left(\frac{8\pi MC_0}{\rho}\right)^{1/2}, \quad (10)$$
$$P_3 = A,$$

where ρ is the density of the Cu deposit and M is its atomic mass, N_0 is the number density of active sites on the electrode surface, and A (s^{-1}) is the nucleation frequency per active site.

The adsorption contribution can be expressed by [31]:

$$j(t)_{\text{ads.}} = P_4 \exp(-P_5 t),$$
$$P_4 = \frac{E}{R_s}, \quad (11)$$
$$P_5 = \frac{1}{R_s C},$$

where E is the applied potential (V), R_s is the solution's resistance (Ω), and C is double layer capacitance (F). Therefore, total contribution to the current density transients shown in Figure 4 is given by:

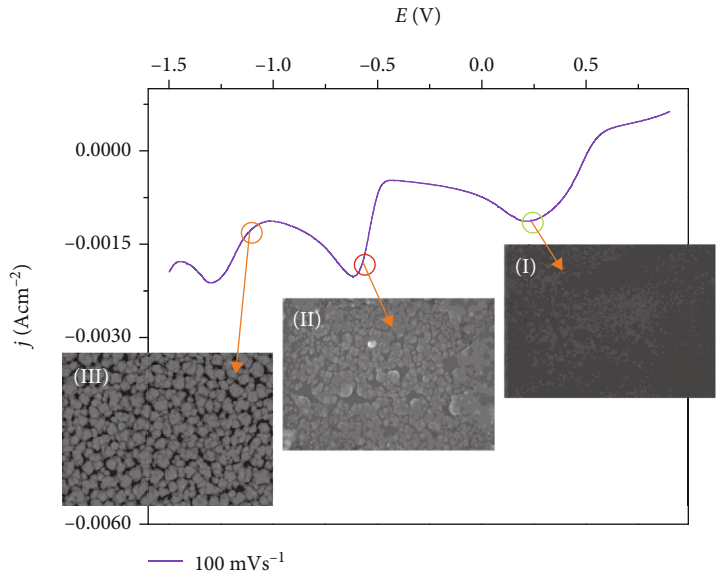

Figure 8: Analysis of GCE surfaces at different applied potentials selected from the CV.

$$j(t)_{\text{total}} = j(t)_{\text{ads.}} + j(t)_{\text{3D}}. \quad (12)$$

Figure 5 displays the comparison between the experimental CAs and the theoretical plots using Eq. (12). The good agreement between these plots means that Eq. (12) is suitable for the description of experimental CAs. Moreover, the derived kinetic parameters, as shown in Table 1, such as A and N_0 are consistent with the trend of metallic nucleation as observed in the literature [24, 30, 34]. Thus, AN_0 product increases with the increase of the potential, confirming the validity of the proposed model. Besides, the average value of the diffusion coefficient, D, is in order $4 \times 10^{-7}\,\text{cm}^2\,\text{s}^{-1}$, which is lower than the result obtained from the CV. However, this is acceptable because it is consistent with several works [24, 29] reported on electrodeposition of other metals in the same DES. Therefore, the use of other methods is necessary as can be seen latter in Cottrell analysis.

To verify the results obtained by CV and Eq. (9), a Cottrell analysis was done to derive the diffusion coefficient from CAs by linearization of longer time after the peak (the falling part) of the transients depicted in Figure 5. Thus, according to the procedure given in to Palomar-Pardave et al. [34] when $t >> t_m$ the transient follows the Cottrell equation (see the red line in the inset of Figure 5), in contrast ($t < t_m$) the CA deviates from that behavior. The diffusion coefficients calculated for the transients of the three peaks are shown in Table 2. It reveals that in general the average values of D are higher than the previous results from the CV and fitting Eq. (9) to experimental data. But they are still in the order and agree with the CV method in the increasing trend of D as the potential becomes more negative.

Applying Eq. (12), it is possible to separate the individual contribution of adsorption and 3D nucleation + diffusion-controlled growth of copper in DES to the total current density transients, as shown in Figure 6. It clearly shows that the current densities corresponding to the adsorption effect (Figure 7(a)) tend to reduce as the potential becomes more negative (increasing in magnitude), while the (peaks) current densities related to $j(t)_{\text{3D}}$ (Figure 7(b)) increase with the applied potentials. These results validate that the use of the proposed model is suitable for the case of copper electrodeposition on the GCE from reline DES.

3.4. SEM and EDS. Figure 8 shows SEM images of GCE surfaces obtained after electrodeposition with the applied potentials corresponding to region associated with different reduction peaks I, II, and III. It reveals clearly that peak I exhibits a surface with the absence of metallic copper, black color, the same color as seen in a bare GCE surface (see Figure 9(a)), while both peaks II and III result in formation of (copper) NPs, which are verified by EDS spectra depicted in the right-hand side of Figures 9(a)–9(c). But it seems to be not efficient using the potentials at peak III due to the hydrogen evolution reaction (see (3)). Moreover, these verify the reduction reactions proposed in the CV analysis. Thus, according to the speciation results and the mechanisms derived from CV and modeling analysis, the nanoparticles observed in Figure 9(c) should be associated with the mixture of $Cu/Cu(OH)_2$ as the core/shell structure due to the presence of OH- ions in (3), as similar to the mechanism of Ni electrodeposition from reline reported in other studies [35, 36]. As suggested from the SEM image depicted in Figure 9(b) showing the formation of metallic (copper) nuclei with different sizes and ages, the copper electrodeposition process onto the GCE from DES containing a small amount of water follows to the progressive nucleation mechanism. This could be explained due to the contribution of the adsorption process, which occurs first in the short time of the CA, giving rise to the formation of the first nuclei on the electrode surfaces.

It is worth mentioning that the Cu-NPs obtained using the potential around peak II are denser than those obtained from peak III giving more porous and larger particle size.

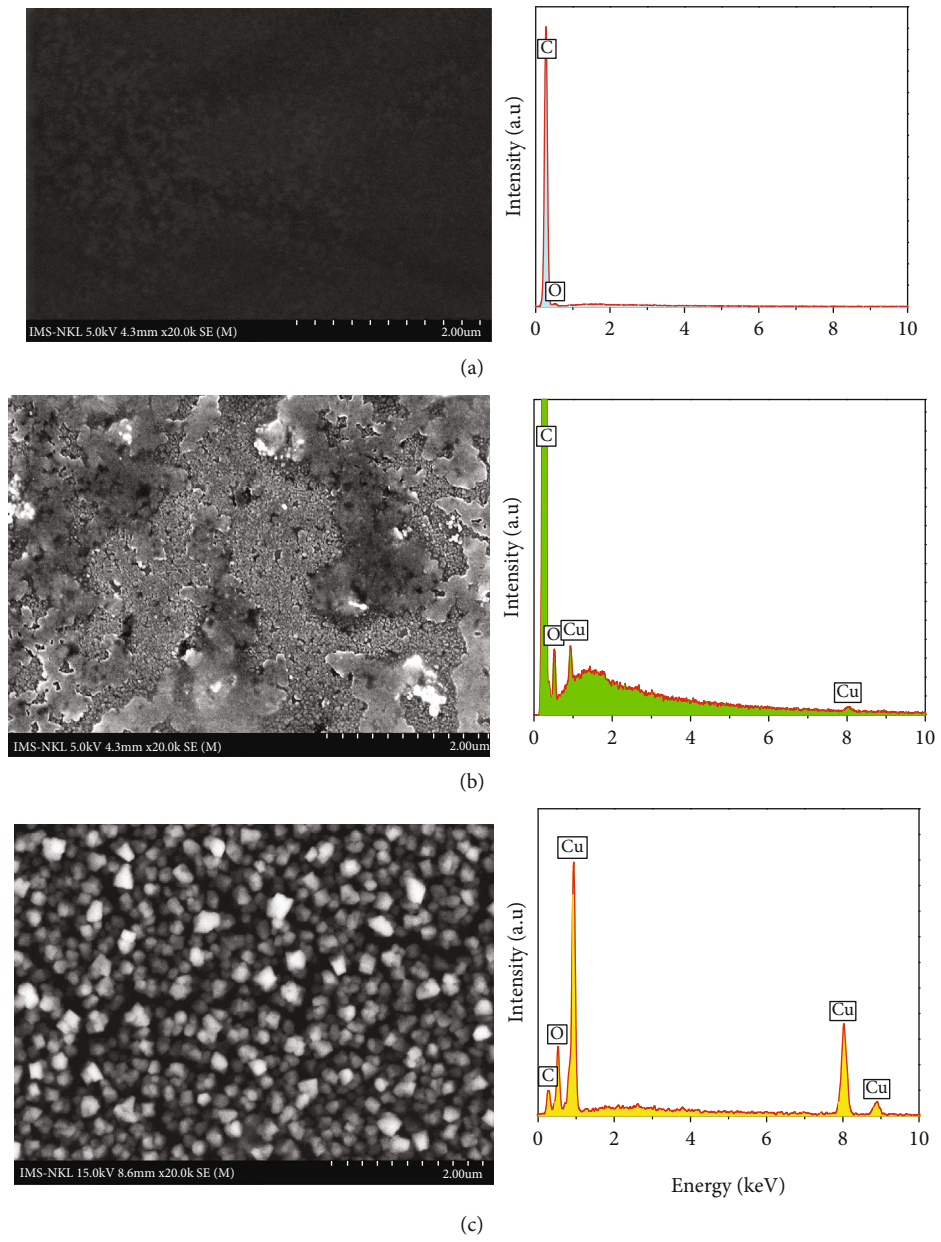

FIGURE 9: SEM images showing Cu-NPs and their corresponding EDS spectra obtained on the GCE surfaces at different reduction peaks using an applied potential of (a) -0.4 V during 3600 s, (b) -0.61 V during 60 s, and (c) -1.1 V during 3600 s at 70°C.

This is extremely useful for further applications (i.e., biosensors, microelectromechanical systems, and MEMS) of the copper electrodeposition from DES since one can select the (appropriate) conditions to obtain desired surface morphology, structure, and chemical composition.

4. Conclusions

The electrochemical synthesis of Cu-NPs from DES reline (containing a small amount of water, ~0.35%) was thoroughly studied. From the UV-Vis spectra measurements, a sudden change in color of Cu^{2+} electrolytes solution from blue to green was observed by heating the solution from room temperature to above 40°C. This can be associated with the presence of complex species such as $[CuCl_n(H_2O)_m]^{(2-x)-}$, where $n + m = 4 - 6$ and $x = 0 - 6$. A wider potential range (compared to the literature) observed from the recorded CV on the system GCE/50 mM Cu(II) in DES, which exhibits more complex behavior with three reduction peaks (see (1), (2), and (3)). By means of the CA technique, it was possible to distinguish the electrochemical behavior of these processes, indicating that peak I corresponds to the reduction of intermediate (soluble) species (Cu(II) to (Cu(I)), (1)); peak II corresponds to the formation of metallic copper from soluble species ((Cu(I)) to Cu(0), (2)), and peak III could be occurring simultaneously both reactions, namely, hydrogen

evolution reaction of small amount of water containing in DES and (2). From these results, it has verified that the copper electrodeposition can be performed by the single potentiostatic step route. A model, comprising two contributions, 3D nucleation and diffusion-controlled growth + adsorption, was proposed and validated to explain the copper electrodeposition on the GCE from the reline DES. These kinetic and mechanistic aspects play the key role in controlling morphology, structure, and chemical composition of Cu-NPs, which are verified by surface characterization techniques using SEM and EDS. Finally, SEM images have verified that the copper electrodeposition from DES containing a small amount of water follows the progressive nucleation mechanism.

Data Availability

The data used to support the findings of this study have not been made available because it is part of an undergoing project.

Conflicts of Interest

The authors declare that they have no conflicts of interest.

Acknowledgments

This research is funded by the Vietnam National Foundation for Science and Technology Development (NAFOSTED) under grant number 103.02-2019.28.

References

[1] M. B. Gawande, A. Goswami, F. X. Felpin et al., "Cu and Cu-based nanoparticles: synthesis and applications in catalysis," *Chemical Reviews*, vol. 116, no. 6, pp. 3722–3811, 2016.

[2] M. I. Din, F. Arshad, Z. Hussain, and M. Mukhtar, "Green adeptness in the synthesis and stabilization of copper nanoparticles: catalytic, antibacterial, cytotoxicity, and antioxidant activities," *Nanoscale Research Letters*, vol. 12, no. 1, p. 638, 2017.

[3] G. Eranna, B. Joshi, D. Runthala, and R. Gupta, "Oxide materials for development of integrated gas sensors—a comprehensive review," *Critical Reviews in Solid State and Materials Sciences*, vol. 29, no. 3-4, pp. 111–188, 2004.

[4] H. M. Zhang, W. Xu, G. Li, Z. M. Liu, Z. C. Wu, and B. G. Li, "Assembly of coupled redox fuel cells using copper as electron acceptors to generate power and its in-situ retrieval," *Scientific Reports*, vol. 21059, 2016.

[5] F. Parveen, B. Sannakki, M. V. Mandke, and H. M. Pathan, "Copper nanoparticles: synthesis methods and its light harvesting performance," *Solar Energy Materials and Solar Cells*, vol. 144, pp. 371–382, 2016.

[6] S. Magdassi, M. Grouchko, and A. Kamyshny, "Copper nanoparticles for printed electronics: routes towards achieving oxidation stability," *Materials (Basel)*, vol. 3, no. 9, pp. 4626–4638, 2010.

[7] D. V. Nguyen, H. M. Nguyen, N. T. Le et al., "Copper nanoparticle application enhances plant growth and grain yield in maize under drought stress conditions," *Journal of Plant Growth Regulation*, pp. 1–12, 2021.

[8] M. T. el-Saadony, M. E. Abd el-Hack, A. E. Taha et al., "Eco-friendly synthesis and insecticidal application of copper nanoparticles against the storage pest Tribolium castaneum," *Nanomaterials (Basel)*, vol. 10, no. 3, p. 587, 2020.

[9] M. Rai, A. P. Ingle, R. Pandit et al., "Copper and copper nanoparticles: role in management of insect-pests and pathogenic microbes," *Nanotechnology Reviews*, vol. 7, no. 4, pp. 303–315, 2018.

[10] E. Masarovicova and K. Kralova, "Metal nanoparticles and plants/nanocząstki metaliczne I rośliny," *Ecological Chemistry and Engineering S*, vol. 20, no. 1, pp. 9–22, 2013.

[11] A. Umer, S. Naveed, N. Ramza, and M. S. Rafique, "Selection of a suitable method for the synthesis of copper nanoparticles," *Nano*, vol. 7, no. 5, p. 1230005, 2012.

[12] P. Huang and Y. Zhang, "Electrodeposition of nickel coating in choline chloride-urea deep eutectic solvent," *International Journal of Electrochemical Science*, vol. 13, pp. 10798–10808, 2018.

[13] A. S. C. Urcezino, L. P. M. dos Santos, P. N. S. Casciano, A. N. Correia, and P. de Lima-Neto, "Electrodeposition study of Ni coatings on copper from choline chloride-based deep eutectic solvents," *Journal of the Brazilian Chemical Society*, vol. 28, no. 7, pp. 1193–1203, 2017.

[14] T. L. Manh, E. M. Arce-Estrada, I. Mej'ıa-Caballero et al., "Iron electrodeposition from Fe(II) ions dissolved in a choline chloride: urea eutectic mixture," *Journal of the Electrochemical Society*, vol. 165, no. 16, pp. D808–D812, 2018.

[15] E. R. Clemente, T. L. Manh, C. E. G. Pano et al., "Aluminum electrochemical nucleation and growth onto a glassy carbon electrode from a deep eutectic solvent," *Journal of the Electrochemical Society*, vol. 166, no. 1, pp. D3035–D3041, 2019.

[16] L. Vieira, A. H. Whitehead, and B. Gollas, "Mechanistic studies of zinc electrodeposition from deep eutectic electrolytes," *Journal of the Electrochemical Society*, vol. 161, no. 1, pp. D7–D13, 2014.

[17] E. L. Smith, A. P. Abbott, and K. S. Ryder, "Deep eutectic solvents (DESs) and their applications," *Chemical Reviews*, vol. 114, no. 21, pp. 11060–11082, 2014.

[18] A. P. Abbott, G. Capper, D. L. Davies, R. K. Rasheed, and V. Tambyrajah, "Novel solvent properties of choline chloride/urea mixtures," *Chemical communications*, no. 1, pp. 70-71, 2003.

[19] A. P. Abbott, K. E. Ttaib, G. Frisch, K. J. McKenzie, and K. S. Ryder, "Electrodeposition of copper composites from deep eutectic solvents based on choline chloride," *Physical Chemistry Chemical Physics*, vol. 11, no. 21, pp. 4269–4277, 2009.

[20] P. Sebastián, E. Vallés, and E. Gómez, "Copper electrodeposition in a deep eutectic solvent. First stages analysis considering Cu(I) stabilization in chloride media," *Electrochimica Acta*, vol. 123, pp. 285–295, 2014.

[21] V. S. Protsenko, A. A. Kityk, D. A. Shaiderov, and F. I. Danilov, "Effect of water content on physicochemical properties and electrochemical behavior of ionic liquids containing choline chloride, ethylene glycol and hydrated nickel chloride," *Journal of Molecular Liquids*, vol. 212, pp. 716–722, 2015.

[22] P. E. Valverde, T. A. Green, and S. Roy, "Effect of water on the electrodeposition of copper from a deep eutectic solvent," *Journal of Applied Electrochemistry*, vol. 50, no. 6, pp. 699–712, 2020.

[23] E. A. M. Cherigui, K. Sentosun, and M. H. Mamme, "On the control and effect of water content during the

electrodeposition of Ni nanostructures from deep eutectic solvents," *The Journal of Physical Chemistry. A*, vol. 122, no. 40, pp. 23129–23142, 2018.

[24] T. D. V. Phuong, L. M. Quynh, N. N. Viet et al., "Effect of temperature on the mechanisms and kinetics of cobalt electronucleation and growth onto glassy carbon electrode using reline deep eutectic solvent," *Journal of Electroanalytical Chemistry*, vol. 880, p. 114823, 2021.

[25] C. Amuli, M. Elleb, J. Meullemeestre, M. J. Schwing, and F. Vierling, "Spectrophotometric study of copper(I1) chloride-trimethyl phosphate solutions. Thermodynamic and spectroscopic properties of copper(II) chloro complexes in nonaqueous solutions," *Inorganic Chemistry*, vol. 25, no. 6, pp. 856–861, 1986.

[26] P. D. Vreese, N. R. Brooks, K. V. Hecke et al., "Speciation of copper(II) complexes in an ionic liquid based on choline chloride and in choline chloride/water mixtures," *Inorganic Chemistry*, vol. 51, no. 9, pp. 4972–4981, 2012.

[27] Q. Zhang, K. D. Vigier, S. Royer, and F. Jerome, "Deep eutectic solvents: syntheses, properties and applications," *Chemical Society Reviews*, vol. 41, pp. 7108–7146, 2012.

[28] T. Berzins and P. Delahay, "Oscillographic polarographic waves for the reversible deposition of metals on solid electrodes," *Journal of the American Chemical Society*, vol. 75, no. 3, pp. 555–559, 1953.

[29] P. Sebastián, E. Torralba, E. Vallés, A. Molina, and E. Gómez, "Advances in copper electrodeposition in chloride excess. A theoretical and experimental approach," *Electrochimica Acta*, vol. 164, pp. 187–195, 2015.

[30] A. M. Popescu, A. Cojocaru, C. Donath, and V. Constantin, "Electrochemical study and electrodeposition of copper(I) in ionic liquid-reline," *Chemical Research in Chinese Universities*, vol. 29, no. 5, pp. 991–997, 2013.

[31] I. Mejıa-Caballero, J. A. Gonzalez, T. L. Manh et al., "Mechanism and kinetics of chromium electrochemical nucleation and growth from a choline chloride/ethylene glycol deep eutectic solvent," *Journal of the Electrochemical Society*, vol. 165, no. 9, pp. D393–D401, 2018.

[32] B. R. Scharifker and J. Mostany, "Three-dimensional nucleation with diffusion controlled growth: part I. Number density of active sites and nucleation rates per site," *Journal of Electroanalytical Chemistry*, vol. 177, no. 1-2, pp. 13–23, 1984.

[33] B. Scharifker and G. Hills, "Theoretical and experimental studies of multiple nucleation," *Electrochimica Acta*, vol. 28, no. 7, pp. 879–889, 1983.

[34] M. Palomar-Pardavé, B. R. Scharifker, E. M. Arce, and M. Romero-Romo, "Nucleation and diffusion-controlled growth of electroactive centers: reduction of protons during cobalt electrodeposition," *Electrochimica Acta*, vol. 50, no. 24, pp. 4736–4745, 2005.

[35] A. Parsa and H. Heli, "Electrodeposition of nickel wrinkled nanostructure from choline chloride:urea deep eutectic solvent (reline) and application for electroanalysis of simvastatin," *Microchemical Journal*, vol. 152, p. 104267, 2020.

[36] J. Aldana-González, M. Romero-Romo, J. Robles-Peralta et al., "On the electrochemical formation of nickel nanoparticles onto glassy carbon from a deep eutectic solvent," *Electrochimica Acta*, vol. 276, pp. 417–423, 2018.